



Cite this: DOI: 10.1039/c6dt04085c

Cyclometalated platinum(II) complexes of 2,2'-bipyridine *N*-oxide containing a 1,1'-bis(diphenylphosphino)ferrocene ligand: structural, computational and electrochemical studies†‡

Hamid R. Shamsavari,^{*a} Masood Fereidoonhezad,^{*b,e} Maryam Niazi,^a S. Talaat Mosavi,^a Sayed Habib Kazemi,^a Reza Kia,^{*c} Shima Shir Khan,^b Siamak Abdollahi Aghdam^a and Paul R. Raithby^d

The preparation and characterization of new heteronuclear-platinum(II) complexes containing a 1,1'-bis(diphenylphosphino)ferrocene (dppf) ligand are described. The reaction of the known starting complex [PtMe(κ^2N,C -bipyO-H)(SMe₂)], **A**, in which bipyO-H is a cyclometalated rollover 2,2'-bipyridine *N*-oxide, with the dppf ligand in a 2 : 1 ratio or an equimolar ratio led to the formation of the corresponding binuclear complex [Pt₂Me₂(κ^2N,C -bipyO-H)₂(μ -dppf)], **1**, or the mononuclear complex [PtMe(κ^1C -bipyO-H)(dppf)], **2**, respectively. According to the reaction conditions, the dppf ligand in **1** and **2** behaves as either a bridging or chelating ligand. All complexes were characterized by NMR spectroscopy. The solid-state structure of **2** was determined by the single-crystal X-ray diffraction method and it was shown that the chelating dppf ligand in this complex was arranged in a "synclinal-staggered" conformation. Also, the occurrence of intermolecular C-H_{Cp}...O_{bipyO-H} interactions in the solid-state gave rise to an extended 1-D network. The electronic absorption spectra and the electrochemical behavior of these complexes are discussed. Density functional theory (DFT) was used for geometry optimization of the singlet states in solution and for electronic structure calculations. The analysis of the molecular orbital (MO) compositions in terms of occupied and unoccupied fragment orbitals in **2** was performed.

Received 24th October 2016,

Accepted 12th January 2017

DOI: 10.1039/c6dt04085c

www.rsc.org/dalton

Introduction

Ever since the serendipitous synthesis of *ferrocene*, numerous derivatives have been prepared.^{1,2} In this regard, ferrocenyl phosphine compounds are a well-known family of ferrocene derivatives that are extensively used in organometallic and

coordination chemistry.^{1–3} One of the most important ferrocenyl phosphine compounds is 1,1'-bis(diphenylphosphino)ferrocene (dppf).^{1,2,4} The dppf is a biphosphine ligand and adopts numerous coordination modes in the complexes of a range of transition metals.^{1–18} These dppf complexes have been utilized in several areas such as catalysis, materials science, electrochemistry, and biology.^{1,2,7,9,10,19–21}

On the other hand, the chemistry of cyclometalated complexes is of great interest because of their use in a wide range of applications.^{22–26} For example, one of the most fascinating classes of cyclometalated complexes is the rollover category.^{27–30} In this family, the cyclometalated moieties are bidentate heterocyclic donors (2,2'-bipyridine (bipy),²⁹ 2,2'-bipyridine *N*-oxide (bipyO)³¹) rather than classical monodentate ligands (2-phenylpyridine (ppy),²⁴ 2-vinylpyridine (vpy)^{32,33}). The bipyO ligand has been by far less explored than the bipy ligand in rollover cyclometalation³¹ or in coordination chemistry.³⁴ The 2,2'-bipyridine *N*-oxide ligand has the two most important possible binding modes in coordination to different metals (Chart 1) which are related to the nature of the central metal.^{31,34}

^aDepartment of Chemistry, Institute for Advanced Studies in Basic Sciences (IASBS), Yousef Sobouti Blvd., Zanjan 45137-6731, Iran. E-mail: shamsavari@iasbs.ac.ir

^bDepartment of Medicinal Chemistry, School of Pharmacy, Ahvaz Jundishapur University of Medical Sciences, Ahvaz, Iran. E-mail: fereidoonhezad-m@ajums.ac.ir

^cChemistry Department, Sharif University of Technology, P.O. Box 11155-3516, Tehran, Iran. E-mail: rkia@sharif.edu

^dDepartment of Chemistry, University of Bath, Claverton Down, Bath, Avon BA2 7AY, UK

^eCancer, Environmental and Petroleum Pollutants Research Center,

Ahvaz Jundishapur University of Medical Sciences, Ahvaz, Iran

† This paper is dedicated to Professor Georg Süss-Fink.

‡ Electronic supplementary information (ESI) available: Full NMR spectra, crystallographic, electrochemistry, computational and molecular simulation details. CCDC 1511315. For ESI and crystallographic data in CIF or other electronic format see DOI: 10.1039/c6dt04085c

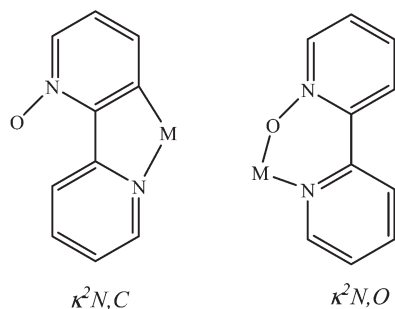


Chart 1 The potential binding modes of the 2,2'-bipyridine *N*-oxide ligand: left, bipyO-H mode and right, bipyO mode.

As part of our ongoing research into the cyclometalation chemistry of platinum,^{32,35–37} we now present the preparation and characterization of new neutral platinum(II) rollover complexes bearing the dppf as a spacer or chelating ligand. Furthermore the optical and electrochemical properties of these complexes are described, the results being supported by theoretical calculations.

Results and discussion

Synthesis and characterization

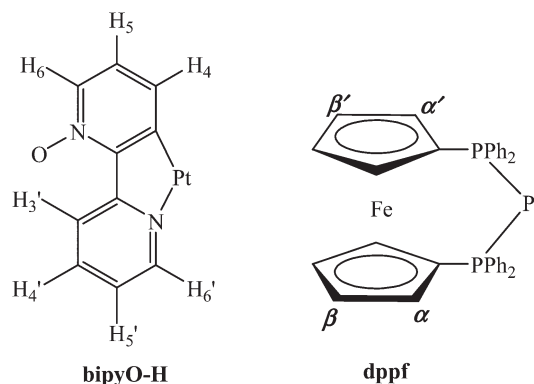
The new chemistry to prepare cycloplatinated(II) rollover complexes is depicted in Scheme 1.

The precursor complex $[\text{PtMe}(\kappa^2N,C\text{-bipyO-H})(\text{SMe}_2)]$, **A**,³¹ in which bipyO-H is a cyclometalated rollover 2,2'-bipyridine *N*-oxide, was prepared by a published method, by reaction of the known dimeric dimethylplatinum(II) complex *cis,cis*- $[\text{PtMe}_2(\mu\text{-SMe}_2)_2\text{PtMe}_2]$ ³⁸ with 2 equivalents of 2,2'-bipyridine *N*-oxide in acetone. Complex **A** was reacted with 0.5 equivalents of the 1,1'-bis(diphenylphosphino)ferrocene (dppf) ligand by replacement of the labile dimethyl sulfide ligand with the phosphorus donor atoms of the dppf ligand. This reaction afforded

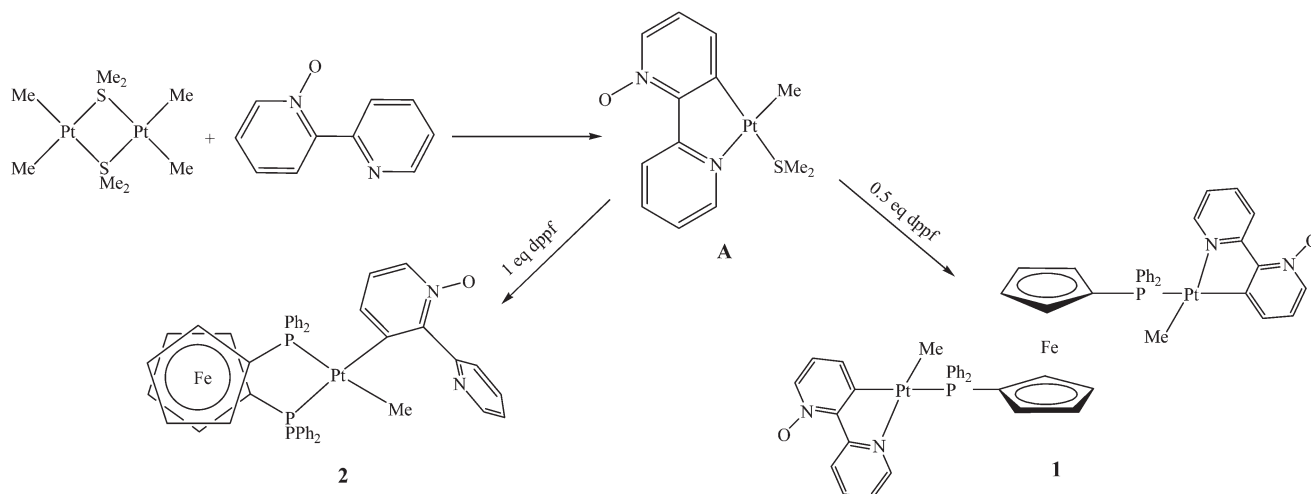
the binuclear complex $[\text{Pt}_2\text{Me}_2(\kappa^2N,C\text{-bipyO-H})_2(\mu\text{-dppf})]$, **1**, which formed as a yellow precipitate. In this complex the dppf ligand adopts an “open bridge” conformation.^{2,5–10} However, when complex **A** was treated with one equivalent of the dppf ligand the Pt–N_{bipyO-H} bond easily dissociated, and the mononuclear complex $[\text{PtMe}(\kappa^1C\text{-bipyO-H})(\text{dppf})]$, **2**, was formed. This bond breaking is related to the potent chelating ability of the dppf ligand due to its large P–P bite angle.² A similar bond cleavage reaction has been observed in analogous cycloplatinated(II) complexes.^{6,10,31,39–41} Complexes **1** and **2** are air-stable and obtained in high yields. They are soluble in halogenated solvents such as CH_2Cl_2 or CHCl_3 and stable for several days at room temperature in solution.

Complexes **1** and **2** were characterized by elemental analyses and their integrity in solution was confirmed by multinuclear NMR spectroscopy (^1H , ^{31}P and ^{195}Pt (CDCl_3)), more details are collected in the Experimental section. The schematic labeling for complexes is shown in Scheme 2.

The structure of binuclear complex **1** was established firstly by ^1H NMR spectroscopy (Fig. S1†). In complex **1** the equivalent methyl signal ($\delta = 0.90$ ppm) is split into a doublet by



Scheme 2 Representative ligands with position labeling.



Scheme 1 The mononuclear and binuclear cycloplatinated(II) rollover complexes containing a dppf ligand.

the ^{31}P nucleus ($^3J_{\text{PH}} = 7.2$ Hz) and there is also splitting of the signal from the ^{195}Pt nucleus ($^2J_{\text{PtH}} = 82.2$ Hz). The platinum coupling constant value confirms that the Me groups are located *trans* to the nitrogen atoms rather than *trans* to the phosphorus atoms.^{6,8} Also, the observation of a single methyl-platinum signal confirms that the two PtMe(bipyO-H) moieties are equivalent.^{6,8} Another useful piece of evidence for confirming this equivalency was the observation of only one low field signal for each of the two $\text{H}^{3'}$ ($\delta = 9.91$ ppm) or H^6 ($\delta = 8.11$ ppm) protons of the pyridyl ring of bipyO-H ligands.^{6–8,31} Moreover, the uncommon chemical shift observed for the $\text{H}^{3'}$ proton is dependent on the orientation of this proton toward the *N*-oxide (N–O) group.^{31,42} The two broad singlet resonances at $\delta = 4.39$ and 4.30 can be assigned to the four α and β protons of the cyclopentadienyl moieties (Cp) of the dppf ligand, respectively. This observation confirmed the equivalency of the two Cp rings in the dppf ligand.^{6–10} The $^{31}\text{P}\{^1\text{H}\}$ NMR spectrum of complex **1** (Fig. S2†) revealed only a singlet signal along with ^{195}Pt satellites at $\delta = 23.3$ ppm with $^1J_{\text{PtP}} = 2307$ Hz, which supports the assignment that both P atoms were equivalent and positioned *trans* to a coordinated carbon atom of the cyclometalated ligand. The $^{195}\text{Pt}\{^1\text{H}\}$ NMR spectrum of complex **1** (Fig. S3†) displayed a doublet at $\delta = -4167$ ppm with $^1J_{\text{PtP}} = 2316$ Hz, which was close to the obtained value from the $^{31}\text{P}\{^1\text{H}\}$ NMR spectrum. Additionally, these observations confirmed that the dppf ligand was symmetrically bridged between the two platinum centers.^{6–10}

The ^1H NMR spectrum of complex **2** was particularly informative and in accordance with the suggested formulation (Fig. S4†). This spectrum exhibited a doublet of doublet resonance for Pt–Me protons at $\delta = 0.03$ ppm which coupled to the platinum center ($^2J_{\text{PtH}} = 65.6$ Hz) and to two different phosphorus atoms ($^3J_{\text{PH}} = 8.7$ and 6.6 Hz) representing the *cis* and

trans coupling constants to the P atoms.^{6,18} The platinum coupling constant value obtained for **2** was significantly lower than the observed value for **1** and it was confirmed that the methyl ligand in complex **2** adopts the *trans* C–Pt–P arrangement. The α and β protons of the dppf ligand appeared as eight broad singlet signals between $\delta = 3.47$ – 4.97 , confirming that all hydrogen atoms of the Cp rings are in different environments, *i.e.* the two Cp moieties are inequivalent. This pattern indicates that the dppf chelate is fairly rigid and adopts the staggered conformation.^{2,6} These data are consistent with the replacement of the nitrogen atom of the cyclometalated ligand by means of the dppf ligand and confirm the high chelating ability of this ligand.² The $^{31}\text{P}\{^1\text{H}\}$ NMR spectrum of complex **2** is shown in Fig. 1, and it confirmed the chelated coordination of the dppf ligand. It displays two distinctive doublets at $\delta = 19.1$ ppm and 23.6 ppm, assigned to the chemically different phosphorus atom donors, with platinum satellites of $^1J_{\text{Pt-P}} = 2191$ Hz (P^{a} atom *trans* to the $\kappa^1\text{C}$ -bipyO-H) and $^1J_{\text{Pt-P}} = 1959$ Hz (P^{b} atom *trans* to the Me), respectively. This result indicates that the methyl ligand exerted a higher *trans* influence than the coordinated carbon atom of the bipyO-H ligand.⁶ As will be shown in the Structural determination section, the Pt– P^{b} bond distance is somewhat longer than that of the Pt– P^{a} bond length. It is interesting to note that perhaps owing to the dppf ligand exerting more strain in its chelating form, the ^{195}Pt coupling constant value (P atom *trans* to the C atom of the cyclometalated ligand) in **2** is noticeably lower than in **1** (acting as a bridging ligand).⁶ Also, in **2** a *cis*-P–P coupling ($^2J_{\text{P}^{\text{a}}\text{P}^{\text{b}}} = 17.2$ Hz) was detected, clearly confirming that the two inequivalent phosphorus atoms couple to each other through the platinum center.^{6,18} Consistent with the $^{31}\text{P}\{^1\text{H}\}$ NMR spectrum, in the $^{195}\text{Pt}\{^1\text{H}\}$ NMR spectrum (Fig. S5†) of **2**, a doublet of doublets was observed at $\delta = -4578$ ppm with $^1J_{\text{PtP}} = 2193$ Hz and 1968 Hz.

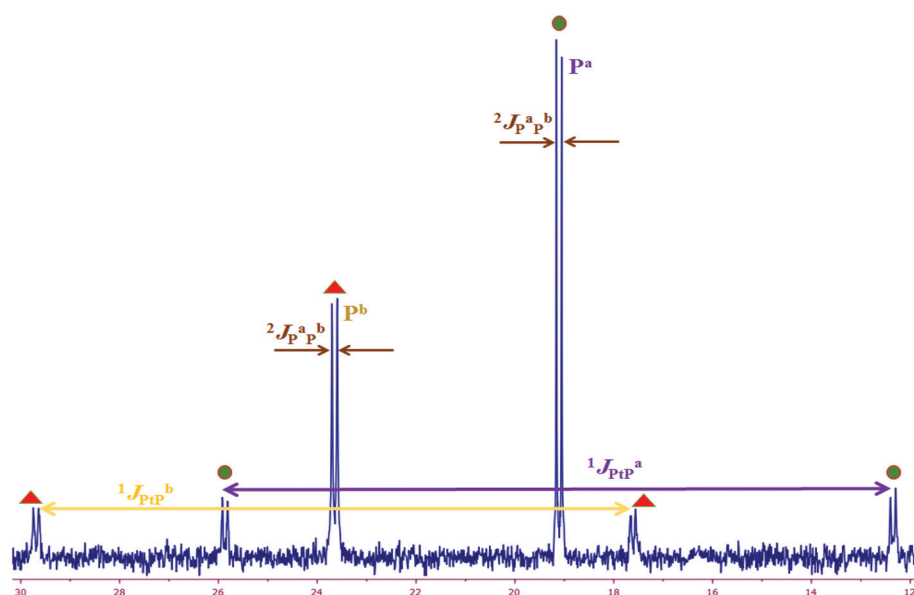


Fig. 1 $^{31}\text{P}\{^1\text{H}\}$ NMR spectrum of complex **2** in CDCl_3 at room temperature.

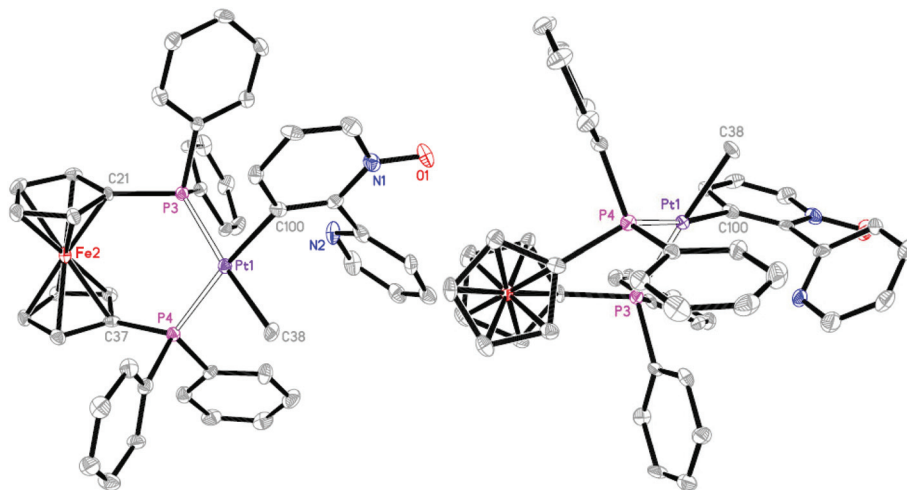


Fig. 2 Two orientations of the unique molecule of **2**, as determined crystallographically, with thermal ellipsoids at the 40% probability level. Hydrogen atoms have been omitted for clarity. Pt(1)–C(100) 2.075(10), Pt(1)–C(38) 2.127(10), Pt(1)–P(3) 2.301(3), Pt(1)–P(4) 2.295(3), P(3)–C(21) 1.803(10), P(4)–C(37) 1.821(11), P(4)–Pt(1)–P(3) 97.96(10), C(100)–Pt(1)–C(38) 85.5(4), C(100)–Pt(1)–P(3) 89.7(3), C(100)–Pt(1)–P(4) 172.0(3), C(38)–Pt(1)–P(3) 175.2(3), C(38)–Pt(1)–P(4) 86.8(3).

Structural determination

The structure of **2** was determined by X-ray crystallography and two views of the molecule are shown in Fig. 2. Crystallographic data are summarized in Table S1.† Complex **2** contains a square planar platinum(II) center with the methyl group, the *ortho* C of the bipyO-H ligand, and two P atoms of the dppf ligand acting as the coordinating atoms. The angles around the Pt center are rather close to the ideal angle of 90°, and this could be contrasted with the strain observed in, for example, organoplatinum complexes containing bis(diphenylphosphino)amine, dppa, as a chelating ligand.⁴³

The imine N is not coordinated and is positioned opposite to the platinum center, and this is in contrast to the usual preference of the bipyO-H ligand to form cyclometalated complexes.³¹ The dppf ligand is arranged in the usually preferred synclinal-staggered conformation.⁴ The Pt(1)–P(3) distance of 2.301(2) Å is longer than the Pt(1)–P(4) distance of 2.295(3) Å, indicating that the methyl ligand probably exerts a higher *trans* influence than the bipyO-κ¹C ligand.³¹ This observation is in agreement with NMR spectroscopic data. On the other hand, the geometry around the metal center is also affected by the intramolecular π⋯π [3.670(6) Å] interaction of the pyridine-*N*-oxide segment and one of the phenyl rings of the dppf ligand.

The interesting feature of the crystal packing of complex **2** is connection of the neighboring molecules into a 1-D extended chain along the *a*-axis by the intermolecular C–H⋯O [C14–H14A⋯O1ⁱ, (i) 1 – *x*, – 1/2 + *y*, 9/2 – *z* and C22–H22A⋯O1ⁱⁱ, (ii) – 1 + *x*, *y*, *z*] hydrogen bonding (Fig. 3).

Optical properties

The UV-vis absorption spectra of all complexes **A**, **1** and **2** were obtained in CH₂Cl₂ at ambient temperature (Fig. 4) and the data are summarized in Table S2.† Also, the electronic absorp-

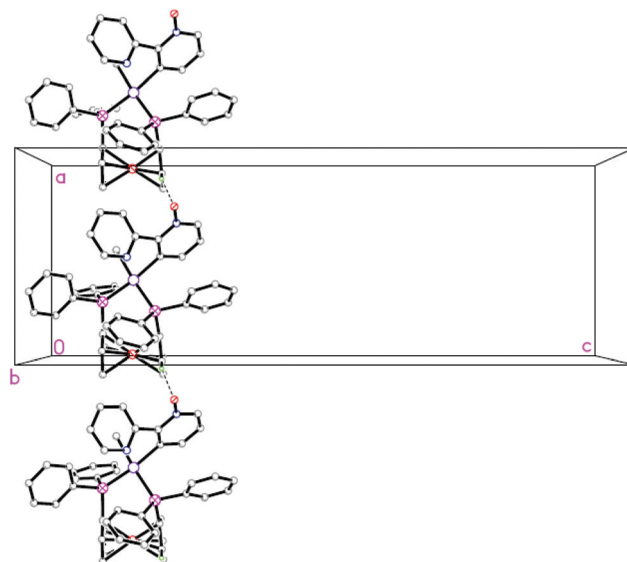


Fig. 3 The crystal packing of **2** viewed down the *b*-axis showing a 1-D extended chain along the *a*-axis by the intermolecular C–H⋯O interactions.

tion spectral data for the dppf ligand^{3,19} are included for comparison.

Complex **A** shows high energy and more intense transitions between 280–320 nm (Table S2.†). These transitions are attributable to the intraligand charge transfer transitions (¹ILCT, π → π*) located on the bipyO-H cyclometalated ligand which are slightly perturbed by coordination to the metal center.^{10,44} The less intense bands at 361 nm and 388 nm are assignable to mixed spin-allowed ¹IL and ¹MLCT transitions (metal to ligand charge transfer).^{32,44} The spectrum of the dppf ligand displays two main absorption bands (Table S2.†). The more intense

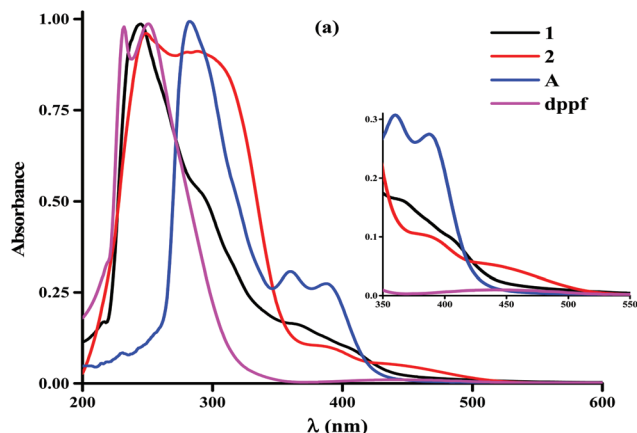


Fig. 4 Electronic absorption spectra of complexes **A**, **1**, **2** and the dppf ligand in CH_2Cl_2 solution (5×10^{-5} M) at room temperature (inset: low energy region).

band at higher energy (in the UV region) is due to the $\pi \rightarrow \pi^*$ transition and the less intense visible absorption band is mostly due to the $^1\text{MLCT}$ transition ($\text{d}(\text{Fe}^{\text{II}}) \rightarrow \pi^*$).^{19,45} Complexes **1** and **2** reveal two main bands with different extinction coefficients (Table S2†). The high energy band in the UV region is remarkably intense and red shifted relative to that of the reported band for complex **A**. This profile can be ascribed to a the $\pi \rightarrow \pi^*$ ($^1\text{ILCT}$) transition which is localized on the bipyO-H cyclometalated and the dppf ligands.^{10,19} While the low intensity bands ($\epsilon = 8.6\text{--}9.2 \text{ M}^{-1} \text{ cm}^{-1}$) in the visible region for **1** are similar to complex **A** with a slight red shift, probably this shift is associated with increasing of contribution of the $^1\text{MLCT}$ transition and the dppf ligand has hardly any influence on these lower energy profiles (Fig. 4).¹⁰ However, in contrast, in **2** the less intense peaks ($\epsilon = 3.4\text{--}6.1 \text{ M}^{-1} \text{ cm}^{-1}$) in this region are admixture transitions and are assignable to $^1\text{L/LCT}$ (ligand to ligand charge transfer, π bipyO-H $\rightarrow \pi^*$ dppf) with a minor contribution of $^1\text{MLCT}$ ($\text{d}(\text{Pt}^{\text{II}}) \rightarrow \text{bipyO-H}$), an assignment which is supported by time-dependent DFT (TD-DFT) calculations (see below).

Computational studies

Electronic structure. The singlet state geometry of complex **2** was optimized in the gas phase using the B3LYP functional of the Gaussian 09 program package.⁴⁶ The molecular orbitals (MO) and singlet excited states of this complex were also studied. The data for the composition of the most important occupied and unoccupied molecular orbitals and the atomic orbital compositions for each complex (%) are listed in Table S3.† The contour plots of the selected important frontier molecular orbitals of **2** are depicted in Fig. S6.† Because of the important role of the frontier molecular orbitals in the electronic excitations and the electronic transition characteristics, it will be useful to map the highest occupied (HOMO) and lowest unoccupied (LUMO) orbitals of **2** on the framework for the excited-state TD-DFT calculations. Therefore, **2** was divided into four segments: the platinum centre (Pt), the methyl group (Me),

the bipyO-H cyclometalating ligand and the dppf ligand. Each part of the percentage contributions is the sum of the atomic orbital coefficient squares. The frontier molecular orbitals (5 occupied MOs and 5 unoccupied MOs) are listed according to their energy and segment contribution. The assignment of each MO was made on the basis of its composition from the segments. The composition of the LUMO is localized on the dppf ligand (π^* character) but the HOMO orbital is mainly localized on the bipyO-H ligand. The HOMO–1 and HOMO–2 orbitals have significant contribution from the Pt metal centre (Table S3†).

Analysis of chemical bonding (extent of donation and back-donation by charge decomposition analysis). The chemical bonding between the platinum center and the ligands in complex **2** can be explained on the basis of donation from the ligands to the metal and π -back-donation from the metal segment to the ligand(s) (σ -donation & π -back-donation) in terms of charge decomposition analysis (CDA) and extended charge decomposition analysis (ECDA).^{47,48} The CDA and Mulliken population analysis (MPA) studies were used to provide better qualitative and quantitative understanding of the chemical bonding in this complex. The procedure for calculating the contributions for each occupied molecular orbital of complex **2**: (i) charge donation through the combination of the occupied orbitals of the ligands and the unoccupied orbitals of the metal segment which can be further split into σ and π donation, (ii) charge π -back-bonding through the combination of the occupied orbitals of the metal segment and the unoccupied orbitals (mostly π^*) of the ligand and (iii) electronic polarization of the metal segment and the ligand. The electronic polarization of fragments is due to the distortion of the electron distribution of the fragments on each other and includes the interactions between all permanent charges and charge multipoles and induced multipoles. The CDA gives reasonable estimates of donation and π -back-donation between the molecular segments only if there is no electronic polarization or it is significantly small. If it is not the case, the difference between the amount of the electron donation and back-donation will not be the same as the net charge transfer between the segments, as calculated from the sum of the atomic charges. Table 1 summarizes some of the properties derived from the charge decomposition analysis of complex **2**. It can be

Table 1 Summary of the computed properties of complex **2**

Property	
%LUFO ^a _{Pt} in OMOs ^c	89.16 (1.78e)
%HOFO ^b _{bipyO-H} in UMOs ^d	35.51 (0.71e)
%HOFO _{dppf} in UMOs	21.39 (0.43e)
Donation (au); Me \rightarrow Pt	0.71e
Donation (au); bipyO-H \rightarrow Pt	0.43e
Donation (au); dppf \rightarrow Pt	0.12e
π -CT ^e (au); Pt \rightarrow bipyO-H	0.05e
π -CT (au); Pt \rightarrow dppf	0.24e

^a LUFO = lowest unoccupied fragment orbital. ^b HOFO = highest occupied fragment orbital. ^c OMOs = occupied molecular orbitals in the complex. ^d UMOs = unoccupied molecular orbitals in the complex. ^e π -Back-donation from the Pt fragment to L.

Table 2 Selected TD-DFT calculated excitation energies and compositions of the lowest-lying singlet excited states for complex **2**

States	E (eV)/ λ (nm)	f	λ_{exp}	Type	Assignment
7	3.92/437	0.05	449	HOMO \rightarrow LUMO (71%) HOMO-1 \rightarrow LUMO (9%)	LL/CT, MLCT
39	4.94/251	0.06	248	HOMO-5 \rightarrow LUMO+1 (33%)	$\pi \rightarrow \pi^*$ (IL)

H and L refer to the highest-occupied and lowest-unoccupied molecular orbitals, respectively.

noted from Table 1 that based on the quantitative data resulting from CDA calculations by AOMix 6.88 software the σ -donation character of the methyl group is greater than the bipyO-H ligand and this is in line with the stronger *trans* influence of the methyl group in lengthening of the opposite bond.

Calculated electronic absorption spectra. TD-DFT calculations were employed to examine the 50 low-lying singlet excited states of complex **2**. The overlay of the experimental and simulated UV-vis spectra of complex **2** is depicted in Fig. S7.† It can be seen that the simulated optical absorption spectra from the TD-DFT calculations reproduce the main features of the experimental spectra. Selected low-lying singlet excited states together with their vertical excitation energies, oscillator strengths and assignment of the transitions for complex **2** are summarized in Table 2. The energy of each excited state is the vertical excitation energy in electron volts from the ground state. The spectral assignment is on the basis of the comparison of experimental band maxima with the calculated energies of the transitions with reasonable oscillator strengths. The excitation of an electron from an occupied to an unoccupied molecular orbital is an experimental model for the excited state (*i.e.*, a one-electron picture). However, the excited states calculated herein demonstrate that excited-state electronic structures are best described in terms of multi-configur-

ations, wherein a linear combination of several occupied-to-unoccupied MO excitations comprises a given optical transition. Assignment of the character of each excited state was based on the compositions of the occupied and unoccupied MOs of the dominant configuration(s) for that excited state. The highest occupied molecular orbital (HOMO) of complex **2** contains contributions from the bipyO-H ligand (91.6% of p orbitals). The HOMO-1 and HOMO-2 are mainly located on the Pt and bipyO-H ligand. On the other hand, the LUMO and LUMO+1 have significant contribution from the dppf ligand. The low-energy calculated absorption band (437 nm) in complex **2** corresponds to excited state S_7 . It is attributed to the charge transfer from the bipyO-H ligand to the dppf ligand and minor charge transfer from the Pt to the bipyO-H ligand (HOMO-1 \rightarrow LUMO contribution). The high-energy absorption band (251 nm) corresponds to excited state 39 and is attributed to the charge transfer from molecular orbitals which are mainly localized on the bipyO-H and the dppf ligands. Electron density difference maps (EDDMs) derived from the TD-DFT calculations were used to show the electron density changes between the ground and excited states upon different electronic excitations. It represents a way for visualizing the electronic distribution, for which one can subtract the ground-state electron density (S_0) from the Franck-Condon electron density of the excited state, thereby providing a picture of the redistribution of the electron density after the vertical transition from the ground-state to any of the Franck-Condon excited states. Visualization of these difference density plots can provide an insight into the subsequent geometric changes occurring on the excited-state potential energy surface, and help to determine what type of excitation is occurring.^{49,50} The electron density difference maps (EDDMs) of complex **2** are shown in Fig. 5, confirming the assignment of the calculated electronic transitions in Table 2.

Electrochemistry. The electrochemical behavior of the free dppf ligand and complexes **1**, **2**, [Pt₂Me₂(κ^2 N,C-ppy)₂(μ -dppf)],

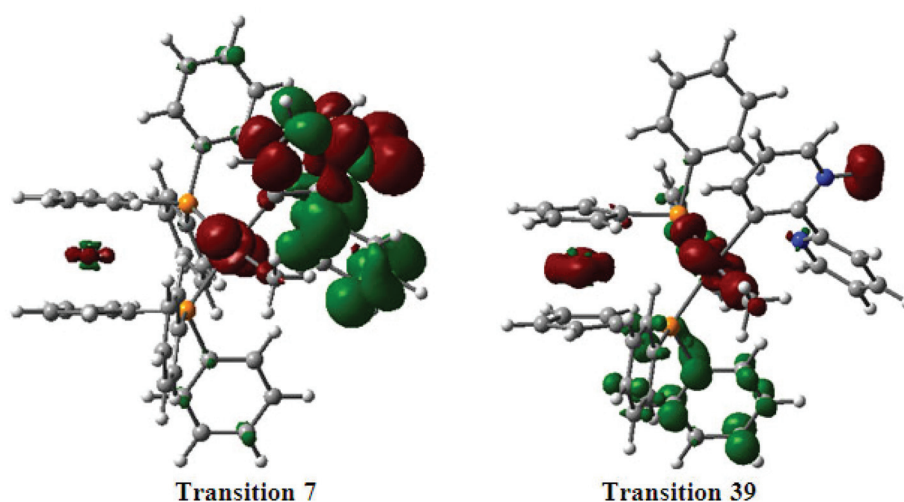


Fig. 5 Electron density difference maps (EDDMs) for the main transitions in complex **2**. Red indicates a decrease in charge transfer, while green indicates an increase.

3,⁶ and [PtMe(κ^1 C-ppy)(dppf)],^{4,6} in which ppy = 2-phenylpyridinyl, between -2.0 and $+2.0$ V vs. reference electrode at a scan rate of 5 mV s^{-1} is presented in Fig. S8[†] (complexes 3 and 4 were selected for comparison purpose). Oxidation and reduction potentials of these complexes are also provided in Table S4.[†]

The dppf ligand oxidation onset is around $+0.5$ V and the peak potential is approximately located at 1.25 V vs. Ag/AgCl.¹⁹ Also, the cyclic voltammogram of the dppf ligand in acetonitrile shows almost irreversible kinetics in which a reduction peak was observed. The complexes containing the dppf ligand in their structure were also investigated by cyclic voltammetry. As shown in Fig. S8,[†] both complexes 1 and 2 show a pair of quasireversible oxidation and reduction peaks which can be assigned to the Pt redox activity. Of course, the oxidation peaks of the dppf ligand and Pt are overlapped but the reduction peaks appearing at approximately -1.25 V originated from the reduction of Pt. It was observed that the oxidation of Pt and the dppf ligand occurs at more positive potentials compared to free Pt or the dppf ligand. Moreover, cyclic voltammograms of complexes 3 and 4 revealed that the oxidation behavior of the dppf ligand occurred at more positive potentials with lower peak currents compared to the free dppf ligand behavior. Additionally, a broad reduction wave was observed for both complexes around -1.0 V which can be attributed to the reduction of Pt. Detailed electrochemical studies of the dppf containing species in the narrower potential range were carried out and it was found that only complexes 1 and 3 display significant electrochemical activity in the range of -1.0 to $+1.0$ V. Fig. 6 depicts the voltammograms of these two complexes.

As seen in Fig. S8,[†] the voltammogram of complex 2 is similar to the electrochemical behavior of the Pt electrode, which may indicate the lower interaction of Pt with the dppf ligand in this complex compared to complex 1. It may suggest

that the dppf group in the structure of complex 2 does not have insignificant changes in its electrochemical behavior. Therefore, for 2 the electrochemistry is relatively similar to the Pt electrochemistry; and may indicate a lower stability of this complex and possible destruction of complex 2 under potential cycling during electrochemical studies. Of course, both complexes 1 and 2 show a broad peak of dppf but in the case of 1 redox peaks of the ferrocene part (Fc) are more distinguishable. Perhaps, in complex 1, the dppf ligand (particularly, the Fc part) becomes more available for electron transfer. On the other hand, the redox behavior of complex 3 is similar to complex 1, especially as seen in Fig. 6 in the potential range of -1.0 V to 1.0 V. The redox behavior of complexes 1–4 seems to be nearly independent of the bipyO-H or ppy groups on their structure.

Conclusion

Dppf is an excellent ligand for the development of a molecular architecture with transition metals. The cycloplatinated complex A was smoothly reacted with the dppf ligand (in varying molar ratios) to produce different products due to the various coordinating abilities of this ligand. When 0.5 equivalents of the dppf ligand were used it acted as a spacer ligand and the dinuclear complex 1 was formed. In contrast, when one molar equivalent of this ligand was applied, the dppf easily displaced the bipyO-H nitrogen to provide the P[^]P chelated mononuclear complex 2; this behavior is related to a large bite angle of dppf. In the crystal structure of 2 the dppf ligand was found to have a synclinal-staggered conformation for the Cp rings. Moreover, this complex showed an interesting hydrogen bond interaction between C–H_{Cp}...O_{bipyO-H} (Fig. 3) generating a one-dimensional network structure in the solid-state. The platinum–phosphorus bond distance for the phosphorus atom *trans* to the coordinated carbon atom of the bipyO-H ligand was slightly shorter than the phosphorus atom *trans* to the methyl ligand. This difference suggests that the κ^1 C-bipyO-H ligand perhaps exerted a lower *trans* influence than the Me ligand. Also, the charge decomposition analyses and molecular orbital diagrams revealed the nature of the compositions of the molecular orbitals of complex 2 based on the fragment analysis and the charge donation and back-donation character of the coordinated ligand. These calculations confirmed the greater *trans* influence of the Me ligand than the C atom of the cyclometalating ligand in complex 2. The UV-vis and electrochemical properties of these complexes have been investigated. The lower energy bands in 1 and 2 were assignable to mixed spin-allowed $^1\text{IL}/^1\text{MLCT}$ or $^1\text{L}'/\text{LCT}/^1\text{MLCT}$ (which is supported by TD-DFT calculations), respectively. Complexes 1 and 2 displayed a pair of quasireversible oxidation and reduction peaks. They could be assigned to the platinum center and the dppf unit. These platinum complexes presented here could thus also potentially be biologically active and the screening of their anticancer behavior is currently under investigation.

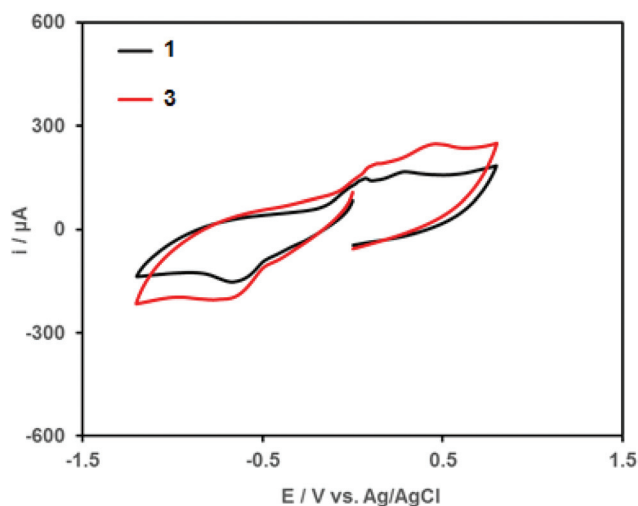


Fig. 6 The cyclic voltammograms of complexes 1 and 3 in 0.05 M LiClO_4 –acetonitrile at a scan rate of 5 mV s^{-1} .

Experimental

All NMR spectra (^1H , ^{31}P { ^1H } and ^{195}Pt { ^1H }) were recorded on a Bruker Avance DPX 400 MHz instrument. References were TMS or the residual peak of the solvent, *i.e.* CDCl_3 (^1H), 85% H_3PO_4 (^{31}P), and aqueous Na_2PtCl_6 (^{195}Pt). The chemical shifts (δ) were reported as ppm and coupling constants (J) expressed in Hz. The microanalyses were performed using a vario EL CHNS elemental analyzer. All solvents were purified and dried according to standard procedures.⁵¹ 2,2'-Bipyridine *N*-oxide and 1,1'-bis(diphenylphosphino)ferrocene were purchased from Aldrich. The precursor complex $[\text{PtMe}(\kappa^2\text{N,C-bipyO-H})(\text{SMe}_2)]$, **A**,³¹ was prepared by the literature method. The NMR labeling for all ligands is shown in Scheme 2 for clarifying the chemical shift assignments.

Synthesis of complexes

$[\text{Pt}_2\text{Me}_2(\kappa^2\text{N,C-bipyO-H})_2(\mu\text{-dppf})]$, **1**. To a solution of complex **A** (100 mg, 0.22 mmol) in acetone (10 mL) was added 0.5 equivalents of dppf (62.5 mg, 0.11 mmol) and the solution was stirred for 2 h at room temperature. A yellow solid was precipitated which was separated and dried under vacuum. Yield: 68%, mp = 253 °C. Anal. Calcd for $\text{C}_{56}\text{H}_{48}\text{FeN}_4\text{O}_2\text{P}_2\text{Pt}_2$ (1317): C, 51.07; H, 3.67; N, 4.25. Found: C, 50.35; H, 3.51; N, 4.09. NMR data in CDCl_3 : $\delta(^1\text{H})$ 0.90 (d, $^2J_{\text{PtH}} = 82.2$ Hz, $^3J_{\text{PH}} = 7.2$ Hz, 6H, 2 Me groups), 4.30 (br s 4H, β and β' of Cp protons), 4.39 (br s, 4H, α and α' of Cp protons), 6.64 (t, $^3J_{\text{HH}} = 6.4$ Hz, 2H, H^5), 7.18 (t, $^3J_{\text{HH}} = 7.3$ Hz, 2H, H^5), 7.33–7.40 (m, 8H, overlapping multiplets), 7.41–7.47 (m, 4H, overlapping multiplets), 7.60 (t, $^3J_{\text{HH}} = 7.4$ Hz, 2H, H^4), 7.63–7.75 (m, 8H, overlapping multiplets), 7.76–7.86 (m, 4H, overlapping multiplets), 8.11 (d, $^3J_{\text{HH}} = 6.2$ Hz, 2H, H^6), 9.91 (d, $^3J_{\text{HH}} = 8.1$ Hz, $^3J_{\text{PH}} = 54.7$ Hz, 2H, H^3); $\delta(^{31}\text{P})$ 23.3 (s, $^1J_{\text{PP}} = 2307$ Hz, 2P of dppf); $\delta(^{195}\text{Pt})$ –4167 (d, $^1J_{\text{PP}} = 2316$, 2Pt).

$[\text{PtMe}(\kappa^1\text{C-bipyO-H})(\text{dppf})]$, **2**. To a solution of complex **A** (100 mg, 0.22 mmol) in acetone (10 mL) was added 1 equivalent of dppf (125 mg, 0.22 mmol) and the solution was stirred for 2 h at room temperature, which produced a yellow solution. After removing of the solvent under reduced pressure, the residue was treated with diethyl ether (2×3 mL). The precipitate as a yellow solid was dried under vacuum. Yield: 78%, mp = 234 °C. Anal. Calcd for $\text{C}_{45}\text{H}_{38}\text{FeN}_2\text{OP}_2\text{Pt}$ (936.7): C, 57.76; H, 4.09; N, 2.99. Found: C, 56.84; H, 3.69; N, 3.08. NMR data in CDCl_3 : $\delta(^1\text{H})$ 0.03 (dd, $^2J_{\text{PtH}} = 65.6$ Hz, $^3J_{\text{PH}} = 8.7$, 6.6 Hz, 3H, 1 Me group), 3.47, 3.53, 3.99 and 4.06 (each br s, 4H, β and β' of Cp protons), 4.19, 4.31, 4.60 and 4.97 (each br s, 4H, α and α' of Cp protons), 6.46 (t, $^3J_{\text{HH}} = 6.9$ Hz, 1H, H^5), 7.01–7.21 (m, 6H, overlapping multiplets), 7.27–7.42 (m, 11H, overlapping multiplets), 7.45–7.52 (m, 3H, overlapping multiplets), 7.56–7.69 (m, 3H, overlapping multiplets), 7.71–7.79 (m, 2H, H^6 , H^6), 8.39 (d, $^3J_{\text{HH}} = 4.4$ Hz, 1H, H^3); $\delta(^{31}\text{P})$ 19.1 (d, $^1J_{\text{PP}} = 2191$ Hz, $^2J_{\text{PP}} = 17.2$ Hz, 1P, P^a atom *trans* to $\kappa^1\text{C-bipyO-H}$), 23.6 (d, $^1J_{\text{PP}} = 1959$ Hz, $^2J_{\text{PP}} = 17.2$ Hz, 1P, P^b atom *trans* to Me); $\delta(^{195}\text{Pt})$ –4578 (dd, $^1J_{\text{PP}} = 2193$ and 1968 Hz, 1Pt).

X-ray crystallography

Single crystals of **2** were suitable for X-ray diffraction analysis and were grown by slow vapor diffusion of *n*-hexane into

CH_2Cl_2 solution of this complex. X-ray intensity data were collected using the full sphere routine by φ and ω scans strategy on the Agilent SuperNova dual wavelength EoS S2 diffractometer with mirror monochromated Mo $\text{K}\alpha$ radiation ($\lambda = 0.71073$ Å). The crystal was cooled to 150 K using an Oxford Diffraction Cryojet low-temperature attachment. The data reduction, including an empirical absorption correction using spherical harmonics, implemented in the SCALE3 ABSPACK scaling algorithm,⁵² was performed using the CrysAlisPro software package.⁵³ The crystal structure was solved by direct methods using the online version of AutoChem 2.0 in conjunction with the OLEX2 suite of programs implemented in the CrysAlis software.^{54,55} The non-hydrogen atoms were refined anisotropically. All of the hydrogen atoms were positioned geometrically in idealized positions and refined with the riding model approximation, with $U_{\text{iso}}(\text{H}) = 1.2$ or $1.5U_{\text{eq}}(\text{C})$. For the molecular graphics the program SHELXTL was used.⁵⁶ All geometric calculations were carried out using the PLATON software.⁵⁷

Computational details

Density functional theory (DFT) calculations have been performed using the Gaussian 09 package to perform geometry optimizations, the vibrational frequencies and the electronic structures of complex **2**.⁴⁶ A frequency calculation after each geometry optimization ensured that the calculated structures are real minima in the potential energy surface of the molecules. The structure of complex **2** was optimized using the B3LYP exchange–correlation functionals with the quasirelativistic Stuttgart–Dresden (SDD) effective core pseudopotential (ECP) and the corresponding set of basic functions for the Pt atom and 6-31G* (five pure d functions) for C, H, N, O, and P.⁵⁸ Molecular orbital (MO) compositions and the overlap populations were calculated using the AOMix 6.88 program.^{59,60} Atomic charges were calculated using the Mulliken population analysis (MPA) as implemented in Gaussian 09. The analysis of the molecular orbital (MO) compositions in terms of the highest occupied orbitals and lowest unoccupied orbitals of the fragment species (HOFOS and LUFOS, respectively) and construction of orbital interaction diagrams were performed by the AOMix 6.88 program. Charge decomposition analysis (CDA) implemented in the AOMix 6.88 program was used to provide better qualitative and quantitative understanding of the nature of the chemical bonding in the complex based on the electron donation and back-donation between the metal and other fragments. Excited singlet states (50 states) were calculated by time-dependent DFT (TD-DFT) in CH_2Cl_2 solvent which was described by using a conductor-like polarizable continuum model (CPCM).⁶¹ The TD-DFT output contained information for the excited-state energies and oscillator strengths (f) and a list of the excitations that gave rise to each excited state, the orbitals involved as well as the wavefunction coefficients of the excitations. From the TD-DFT calculations the electronic distribution and the localization of the singlet excited states were visualized using electron density difference maps (EDDMs).⁶²

GaussSum3 was used for EDDM calculations and for the electronic spectrum simulation.⁶³

Electrochemistry

Cyclic voltammetry (CV) measurements were performed in a three-electrode cell using an Autolab101 potentiostat (Eco-Chemie, The Netherlands). In this system, the platinum electrode and Ag/AgCl electrodes were employed as counter and reference electrodes, respectively. All complexes **1–4** and the dppf ligand were introduced into the structure of a carbon paste electrode for electrochemical investigations. Cyclic voltammograms of the complexes were recorded at room temperature in acetonitrile containing 0.05 M lithium perchlorate (LiClO₄) as a supporting electrolyte under an inert nitrogen atmosphere. The electrochemistry of complexes **1–4** and the dppf ligand was studied in different potential windows. At first, cyclic voltammograms were recorded between +2.0 and –2.0 V at different scan rates. Then, the electrochemical properties were studied in a narrower potential window (–1.0 V to +1.0 V).

Acknowledgements

This work was supported by the Institute for Advanced Studies in Basic Sciences (IASBS) Research Council and the Iran National Science Foundation (Grant No. 95822524). Collaboration of Medicinal Chemistry, Faculty of Pharmacy, Ahvaz Jundishapur University of Medical Sciences, in providing the required facilities for this work is greatly acknowledged. RK is thankful to the Sharif University of Technology research Council for the research facility. RK also thanks Prof. Paul R. Raithby and Bath University for their support. PRR is grateful to the Engineering and Physical Sciences Research Council (EPSRC) for continued funding (EP/K004956/1). Thanks are also due to Mr A. Biglari, the operator of the Bruker NMR instrument at IASBS, for recording the NMR spectra.

References

- 1 A. Togni and T. Hayashi, *Ferrocenes: Homogeneous Catalysis, Organic Synthesis, Materials Science*, Wiley-VCH Verlag GmbH, 1995.
- 2 P. Štěpnička, *Ferrocenes: Ligands, Materials and Biomolecules*, John Wiley & Sons, Ltd, 2008.
- 3 D. A. Khobragade, S. G. Mahamulkar, L. Pospíšil, I. Císařová, L. Rulišek and U. Jahn, *Chem. – Eur. J.*, 2012, **18**, 12267–12277.
- 4 G. Bandoli and A. Dolmella, *Coord. Chem. Rev.*, 2000, **209**, 161–196.
- 5 M. Golbon Haghighi, S. M. Nabavizadeh, M. Rashidi and M. Kubicki, *Dalton Trans.*, 2013, **42**, 13369–13380.
- 6 S. Jamali, S. M. Nabavizadeh and M. Rashidi, *Inorg. Chem.*, 2008, **47**, 5441–5452.
- 7 S. M. Nabavizadeh, H. Amini, H. R. Shahsavari, M. Namdar, M. Rashidi, R. Kia, B. Hemmateenejad, M. Nekoeinia, A. Ariafard, F. Niroomand Hosseini, A. Gharavi, A. Khalafi-Nezhad, M. T. Sharbati and F. Panahi, *Organometallics*, 2011, **30**, 1466–1477.
- 8 S. M. Nabavizadeh, M. Dadkhah Aseman, B. Ghaffari, M. Rashidi, F. Niroomand Hosseini and G. Azimi, *J. Organomet. Chem.*, 2012, **715**, 73–81.
- 9 H. Samouei, M. Rashidi and F. W. Heinemann, *J. Organomet. Chem.*, 2011, **696**, 3764–3771.
- 10 F. Zheng, A. T. Hutton, C. G. C. E. van Sittert, W. J. Gerber and S. F. Mapolie, *Dalton Trans.*, 2015, **44**, 1969–1981.
- 11 S. Pazireh, R. Aghakhanpour Babadi and A. R. Esmailbeig, *J. Organomet. Chem.*, 2016, **803**, 73–81.
- 12 A. Houlton, D. M. P. Mingos, D. M. Murphy, D. J. Williams, L.-T. Phang and T. S. A. Hor, *J. Chem. Soc., Dalton Trans.*, 1993, 3629–3630.
- 13 M. C. Gimeno, A. Laguna, C. Sarroca and P. G. Jones, *Inorg. Chem.*, 1993, **32**, 5926–5932.
- 14 A. Acosta-Ramírez, M. Muñoz-Hernández, W. D. Jones and J. J. García, *J. Organomet. Chem.*, 2006, **691**, 3895–3901.
- 15 O. Crespo, M. C. Gimeno and A. Laguna, *Appl. Organomet. Chem.*, 2000, **14**, 644–652.
- 16 F. Canales, M. C. Gimeno, P. G. Jones, A. Laguna and C. Sarroca, *Inorg. Chem.*, 1997, **36**, 5206–5211.
- 17 D. Giardina-Papa, I. Ara, S. Ibáñez, P. Mastorilli, V. Gallo and J. Forníes, *Polyhedron*, 2016, **120**, 44–53.
- 18 H. R. Shahsavari, M. Rashidi, S. M. Nabavizadeh, S. Habibzadeh and F. W. Heinemann, *Eur. J. Inorg. Chem.*, 2009, 3814–3820.
- 19 A. Diez, J. Fernandez, E. Lalinde, M. T. Moreno and S. Sanchez, *Dalton Trans.*, 2008, 4926–4936.
- 20 Y. Hokai, B. Jurkovic, J. Fernández-Gallardo, N. Zakirkhodjaev, M. Sanaú, T. R. Muth and M. Contel, *J. Inorg. Biochem.*, 2014, **138**, 81–88.
- 21 J. F. Hartwig, *Inorg. Chem.*, 2007, **46**, 1936–1947.
- 22 M. Albrecht, *Chem. Rev.*, 2009, **110**, 576–623.
- 23 Y. Chi and P.-T. Chou, *Chem. Soc. Rev.*, 2010, **39**, 638–655.
- 24 I. Omae, *Cyclometalation Reactions: Five-Membered Ring Products as Universal Reagents*, Springer, 2014.
- 25 W.-Y. Wong and C.-L. Ho, *Acc. Chem. Res.*, 2010, **43**, 1246–1256.
- 26 G. Zhou, W.-Y. Wong, S.-Y. Poon, C. Ye and Z. Lin, *Adv. Funct. Mater.*, 2009, **19**, 531–544.
- 27 B. Butschke and H. Schwarz, *Chem. Sci.*, 2012, **3**, 308–326.
- 28 B. Butschke, M. Schlangen, D. Schröder and H. Schwarz, *Chem. – Eur. J.*, 2008, **14**, 11050–11060.
- 29 A. Zucca, G. L. Petretto, S. Stoccoro, M. A. Cinellu, M. Manassero, C. Manassero and G. Minghetti, *Organometallics*, 2009, **28**, 2150–2159.
- 30 L. Maidich, G. Dettori, S. Stoccoro, M. A. Cinellu, J. P. Rourke and A. Zucca, *Organometallics*, 2015, **34**, 817–828.
- 31 M. E. Moustafa, P. D. Boyle and R. J. Puddephatt, *Organometallics*, 2014, **33**, 5402–5413.

- 32 M. Niazi and H. R. Shahsavari, *J. Organomet. Chem.*, 2016, **803**, 82–91.
- 33 A. Zucca, L. Maidich, V. Carta, G. L. Petretto, S. Stoccoro, M. Agostina Cinellu, M. I. Pilo and G. J. Clarkson, *Eur. J. Inorg. Chem.*, 2014, **2014**, 2278–2287.
- 34 O. Toma, N. Mercier, M. Allain, A. Forni, F. Meinardi and C. Botta, *Dalton Trans.*, 2015, **44**, 14589–14593.
- 35 M. Niazi and H. R. Shahsavari, *ChemistrySelect*, 2016, **1**, 1780–1783.
- 36 M. Niazi, H. R. Shahsavari, M. Golbon Haghighi, M. R. Halvagar, S. Hatami and B. Notash, *RSC Adv.*, 2016, **6**, 76463–76472.
- 37 M. Niazi, H. R. Shahsavari, M. Golbon Haghighi, M. R. Halvagar, S. Hatami and B. Notash, *RSC Adv.*, 2016, **6**, 95073–95084.
- 38 J. D. Scott and R. J. Puddephatt, *Organometallics*, 1983, **2**, 1643–1648.
- 39 M. Golbon Haghighi, M. Rashidi, S. M. Nabavizadeh, S. Jamali and R. J. Puddephatt, *Dalton Trans.*, 2010, **39**, 11396–11402.
- 40 L. Maidich, G. Zuri, S. Stoccoro, M. A. Cinellu and A. Zucca, *Dalton Trans.*, 2014, **43**, 14806–14815.
- 41 A. R. Esmaeilbeig, M. Golbon Haghighi, S. Nikahd, S. Hashemi, M. Mosarezaee, M. Rashidi and S. M. Nabavizadeh, *J. Organomet. Chem.*, 2014, **755**, 93–100.
- 42 R. Puttreddy, O. Jurcek, S. Bhowmik, T. Makela and K. Rissanen, *Chem. Commun.*, 2016, **52**, 2338–2341.
- 43 S. J. Hoseini, M. Mohamadikish, K. Kamali, F. W. Heinemann and M. Rashidi, *Dalton Trans.*, 2007, 1697–1704.
- 44 M. Jamshidi, S. M. Nabavizadeh, H. R. Shahsavari and M. Rashidi, *RSC Adv.*, 2015, **5**, 57581–57591.
- 45 B. J. Coe, S. P. Foxon, R. A. Pilkington, S. Sánchez, D. Whittaker, K. Clays, G. Depotter and B. S. Brunshwig, *Organometallics*, 2015, **34**, 1701–1715.
- 46 M. J. Frisch, G. W. Trucks, H. B. Schlegel, G. E. Scuseria, M. A. Robb, J. R. Cheeseman, G. Scalmani, V. Barone, B. Mennucci, G. A. Petersson, H. Nakatsuji, M. Caricato, X. Li, H. P. Hratchian, A. F. Izmaylov, J. Bloino, G. Zheng, J. L. Sonnenberg, M. Hada, M. Ehara, K. Toyota, R. Fukuda, J. Hasegawa, M. Ishida, T. Nakajima, Y. Honda, O. Kitao, H. Nakai, T. Vreven, J. J. A. Montgomery, J. E. Peralta, F. Ogliaro, M. Bearpark, J. J. Heyd, E. Brothers, K. N. Kudin, V. N. Staroverov, T. Keith, R. Kobayashi, J. Normand, K. Raghavachari, A. Rendell, J. C. Burant, S. S. Iyengar, J. Tomasi, M. Cossi, N. Rega, J. M. Millam, M. Klene, J. E. Knox, J. B. Cross, V. Bakken, C. Adamo, J. Jaramillo, R. Gomperts, R. E. Stratmann, O. Yazyev, A. J. Austin, R. Cammi, C. Pomelli, J. W. Ochterski, R. L. Martin, K. Morokuma, V. G. Zakrzewski, G. A. Voth, P. Salvador, J. J. Dannenberg, S. Dapprich, A. D. Daniels, O. Farkas, J. B. Foresman, J. V. Ortiz, J. Cioslowski and D. J. Fox, *Gaussian 09, Revision B.01*, 2010.
- 47 S. I. Gorelsky, S. Ghosh and E. I. Solomon, *J. Am. Chem. Soc.*, 2006, **128**, 278–290.
- 48 S. I. Gorelsky and E. I. Solomon, *Theor. Chem. Acc.*, 2008, **119**, 57–65.
- 49 G. T. Burdzinski, T. L. Gustafson, J. C. Hackett, C. M. Hadad and M. S. Platz, *J. Am. Chem. Soc.*, 2005, **127**, 13764–13765.
- 50 K. B. Wiberg, C. M. Hadad, C. M. Breneman, K. E. Laidig, M. A. Murcko and T. J. Lepage, *Science*, 1991, **252**, 1266–1272.
- 51 B. S. Furniss, A. J. Hannaford, P. W. G. Smith and A. R. Tatchell, *Vogel's Textbook of Practical Organic Chemistry*, Longman Scientific & Technical, 5th edn, 1989.
- 52 R. C. Clark and J. S. Reid, *Acta Crystallogr., Sect. A: Fundam. Crystallogr.*, 1995, **51**, 887–897.
- 53 SuperNova Eos S2 System: Empirical absorption correction, 2011, CrysAlis-Software package, Oxford Diffraction Ltd.
- 54 O. V. Dolomanov, L. J. Bourhis, R. J. Gildea, J. A. K. Howard and H. Puschmann, *J. Appl. Crystallogr.*, 2009, **42**, 339–341.
- 55 Agilent, *AutoChem 2.0, in conjunction with OLEX2*, Agilent Technologies UK Ltd, Yarnton, Oxfordshire, England, 2012.
- 56 A. Spek, *Acta Crystallogr., Sect. D: Biol. Crystallogr.*, 2009, **65**, 148–155.
- 57 G. Sheldrick, *Acta Crystallogr., Sect. A: Fundam. Crystallogr.*, 2008, **64**, 112–122.
- 58 D. Andrae, U. Häußermann, M. Dolg, H. Stoll and H. Preuß, *Theor. Chim. Acta*, 1990, **77**, 123–141.
- 59 S. I. Gorelsky and A. B. P. Lever, *J. Organomet. Chem.*, 2001, **635**, 187–196.
- 60 S. I. Gorelsky, *AOMix program*, <http://www.sg-chem.net/>.
- 61 M. Cossi and V. Barone, *J. Chem. Phys.*, 2001, **115**, 4708–4717.
- 62 W. R. Browne, N. M. O'Boyle, J. J. McGarvey and J. G. Vos, *Chem. Soc. Rev.*, 2005, **34**, 641–663.
- 63 N. M. O'Boyle, A. L. Tenderholt and K. M. Langner, *J. Comput. Chem.*, 2008, **29**, 839–845.